IEEE Access
Multidisciplinary | Rapid Review | Open Access Journal

Received August 18, 2021, accepted August 28, 2021, date of publication August 30, 2021, date of current version September 7, 2021.

Digital Object Identifier 10.1109/ACCESS.2021.3109141

Adaptive Terminal Sliding Mode Based Load Frequency Control for Multi-Area Interconnected Power Systems With PV and Energy Storage

ZHENGHAO WANG AND YONGHUI LIU
School of Electrical Engineering, Shanghai Dianji University, Shanghai 201306, China
Corresponding author: Yonghui Liu (liuyh@sdju.edu.cn)

This work was supported in part by the National Natural Science Foundation of China under Grant 61803253.

ABSTRACT In this paper, the load frequency control problem of multi-area interconnected power systems containing PV and energy storage system is considered. First, based on the traditional load frequency control model, the model of photovoltaic and energy storage system is established. Then, when the upper and lower bounds of disturbances are known, a fast terminal sliding mode controller is designed, which compensates the influence of disturbances effectively. Further, by introducing an adaptive law to estimate the bound of the unknown disturbances, an adaptive fast terminal sliding mode controller is designed, which reduces the dependence on the disturbance boundary. By designing the controller, the stability of the system is analyzed. Finally, simulations are performed with two area power systems to verify the effectiveness of the designed controller. The simulation results show that the adaptive fast terminal sliding mode controller can overcome the effects of disturbances. In addition, when the energy storage system and the controller participate in frequency regulation, the load frequency deviation fluctuation is further reduced, which enhances the performance of system.

INDEX TERMS Multi-area interconnected power systems, load frequency control, terminal sliding mode control, adaptive control.

I. INTRODUCTION

In recent years, with the increasingly serious situation of global warming, concerns about energy security and anxiety about environmental degradation have deepened, making full use of renewable energy has become global consensus. Grid-connected power generation from large-scale renewable energy sources, represented by solar and wind power, has become an unstoppable trend for new power systems. Among them, solar energy is widely used due to its advantage of large storage capacity, wide distribution and *positive peaking* [1]. However, with the increasing penetration of renewable energy generation in the power systems, the frequency modulation ability of the traditional generators is failed to satisfy the requirements. Meanwhile, the continuous development of grid technology has further strengthened grid connections between different areas, which forms the multi-area interconnected power systems [2]–[4]. With the more complex power conditions, the requirements of load frequency control (LFC) in interconnected power systems have been gradually increased.

To cope with the impact of failures in power equipment and changes in load demand on system operation, the installation of energy storage systems (ESS) in power systems has been found to be an effective method. ESS can respond quickly in load frequency changes of the power systems. Many researches have been focused on power systems with ESS. Combined with the energy storage joint frequency modulation project of the Southern China Power Grid, the energy storage joint frequency regulation can improve the frequency regulation performance index of generators is verified in [5]. In [6], the interconnected power systems containing supercapacitors is considered. The Buck-Boost structure and fuzzy control strategy are proposed to control the charging and discharging of supercapacitors, thereby achieving the index of LFC. A hybrid energy storage system consisting of supercapacitors and fuel cells is considered in [7], which combined neural networks with adaptive control to achieve LFC in multi-area interconnected power systems. In [8], the cases containing superconducting magnetic and capacitive energy

The associate editor coordinating the review of this manuscript and approving it for publication was Engang Tian.

storage models are considered. A model predictive controller is designed to implement LFC for three-area interconnected power systems. In [9], the energy storage of idle electric vehicles is fully utilized. To address the possible cyber-attacks during grid connection of electric vehicles [10], a memory-based event-triggered H∞ LFC method is proposed. Although the above research results have achieved LFC for systems containing energy storage, the renewable energy generation connected to the grid has not been considered. In [11], the inherent uncertainty of renewable energy generation systems and the interconnection of area power systems are considered. The pumped storage power plants are used as the energy storage part of the system. By designing the fractional-order PID controller, the LFC of the interconnected power systems is implemented. An optimization scheme for the controller is focused on in [12]. By proposing a new control method with variable structure gain scheduling, the advantages of different PI controllers are integrated. The control of the load frequency is achieved and the performance of the system operation is further improved. As the power systems structure becomes more complex, more efficient control strategies are needed for power systems.

Notably, in order to adjust the energy structure, the penetration rate of renewable energy generation in the power systems is increasing. If only relying on the ESS to modulate the frequency deviation, it is necessary to allocate large capacity storage devices, which will increase the construction cost of the power systems. To reduce the cost of grid construction and improve the system stability effectively, this paper utilizes the ESS and sliding mode controller (SMC) in cooperative mode. SMC has better robustness for external disturbances and internal parameter variations of the system, which are also easy to realize in engineering. For example, in order to suppress the load frequency deviation of the interconnected system containing wind power, a hybrid control method based on fuzzy logic and nonlinear sliding mode control is proposed in [13]. A case containing wind power and ESS is considered in [14]. A coordination control strategy for the sliding model load frequency controller and ESS is proposed. However, compared with the traditional SMC, terminal sliding mode controller (TSMC) has shorter convergence time and the inherent jitter phenomenon is not obvious, which improves the system performance. In addition, the TSMC enables the system to converge to the equilibrium point in finite time, which further improves the convergence speed. Thus, many researches have been focused on robots [15], electric motors [16], and rail transportation [17], [18]. For power systems, to achieve tracking of the maximum power point for PV systems, a TSMC is designed in [19]. In [20], the grid-connected wind power is considered. The LFC of the system with generation constraints is achieved by designing TSMC. Faced with the systems containing renewable energy sources and ESS, TSMC is designed and optimized by artificial bee colony algorithm in [21], which achieved the control objectives of LFC. However, the researches of single area operation in [20], [21] cannot longer satisfy the requirements of power systems development. Further studies are needed to deal with the LFC problem for multiple area interconnections.

Based on the above analysis, LFC of interconnected power systems has been researched with energy storage devices. However, the renewable energy sources connected to the grid, such as PV are not considered. In addition, LFC has been researched by the improved PID and other control methods. However, the algorithm is complex that it is not convenient to implement in engineering. In contrast, the SMC has good robustness to external disturbances. Moreover, it can speed up the convergence of the system.

Motivated by the above discussions, the contributions of this work are specified as follows:

i. In order to solve the influence of PV generation uncertainty on load frequency deviation, a LFC model of interconnected power systems containing PV and ESS is proposed in this paper.
ii. Based on proposed LFC model containing PV and ESS, a TSMC is designed to reduce the load frequency deviation of interconnected power systems.
iii. By introducing the adaptive law to estimate the upper bound of the disturbances, the adaptive terminal sliding mode controller is designed to reduce the dependence on disturbances boundary.

The subsequent sections of this paper are organized as follows: Section 2 presents the system model. In Section 3, we focus on the stability analysis. Section 4 develops the simulation verification of the designed controller. Combining the simulation results and analysis, we summarize the conclusions in Section 5.

II. SYSTEM MODEL DESCRIPTION

In this paper, based on the traditional LFC model, the LFC model of multi-area interconnected power systems containing PV and ESS is constructed. Further, the adaptive fast terminal sliding mode controller is designed to work with the energy storage device cooperatively, which reduces the deviation of frequency during the operation of the power systems. The description of each part in the model is given as follows.

A. LFC MODEL INCLUDING PV AND ESS

For convenience of analysis, under stable operation of the power systems, it is supposed that one generator is used to represent the overall performance of the generator set in the model built. This paper mainly analyzes LFC of power systems containing PV and ESS. Therefore, the phenomenon of time delay in the signal transmission process can be ignored. Based on the above assumptions, the model including PV and ESS is shown in Fig. 1.

B. LFC MODEL INCLUDING PV AND ESS

The transfer function of the PV system is expressed as follows [22]:

$$G_{\mathrm{pv}i}(s) = \frac{k_{\mathrm{p}i}}{\lambda_{1i} + s} \cdot \frac{\lambda_{2i} + s}{\lambda_{3i} + s} \tag{1}$$

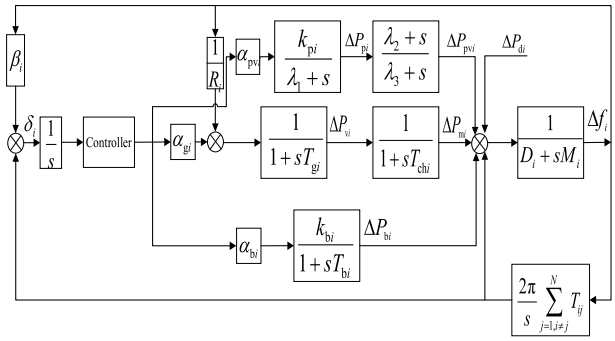

FIGURE 1. LFC model including PV and ESS.

where k_{pi} is PV gain factor, λ_{1i} and λ_{3i} are the opposite of the transfer function's polar horizontal coordinates, respectively. λ_{2i} is the opposite of the transfer function's zero horizontal coordinate.

Further, the PV output power is expressed as

$$\Delta\dot{P}_{\mathrm{p}i} = -\lambda_{1i}\Delta P_{\mathrm{p}i} + k_{\mathrm{p}i}\alpha_{\mathrm{pv}i}u(t) \tag{2}$$

$$\Delta\dot{P}_{\mathrm{pv}i} = -\lambda_{3i}\Delta P_{\mathrm{pv}i} + (\lambda_{2i} - \lambda_{1i})\Delta P_{\mathrm{p}i} - k_{\mathrm{p}i}\alpha_{\mathrm{pv}i}u(t) \tag{3}$$

where $\alpha_{\mathrm{pv}i}$ is PV proportional factor, $u(t)$ is control input.

By exchanging active power with grid, the frequency control function of ESS is achieved. When the ESS is used for frequency control, a certain response time is required to control its charging and discharging process. Therefore, a first-order inertial segment is used to describe the process, the ESS output power is expressed as:

$$\Delta\dot{P}_{\mathrm{b}i} = -\frac{1}{T_{\mathrm{b}i}}\Delta P_{\mathrm{b}i} + \frac{\alpha_{\mathrm{b}i}k_{\mathrm{b}i}}{T_{\mathrm{b}i}}u(t) \tag{4}$$

where $\Delta P_{\mathrm{b}i}$ is deviation of ESS output power, $k_{\mathrm{b}i}$ is ESS gain factor, $T_{\mathrm{b}i}$ is ESS time instants, R_i is governor speed regulation, $\alpha_{\mathrm{b}i}$ is ESS proportional factor.

C. THERMAL POWER UNIT MODEL

The governor is an important part of the prime mover. By switching on/off of the steam gate, the control of the power entering the prime mover and distributes the load among the units are realized. The governor is expressed as:

$$\Delta\dot{P}_{\mathrm{v}i} = -\frac{1}{R_i T_{\mathrm{g}i}}\Delta f_i - \frac{1}{T_{\mathrm{g}i}}\Delta P_{\mathrm{v}i} + \frac{\alpha_{\mathrm{g}i}}{T_{\mathrm{g}i}}u(t) \tag{5}$$

where Δf_i is frequency deviation, $\Delta P_{\mathrm{v}i}$ is control valve position deviation, $T_{\mathrm{g}i}$ is governor time constant, $\alpha_{\mathrm{g}i}$ is turbine proportional factor.

The turbine power output are as follows:

$$\Delta\dot{P}_{\mathrm{m}i} = -\frac{1}{T_{\mathrm{ch}i}}\Delta P_{\mathrm{m}i} + \frac{1}{T_{\mathrm{ch}i}}\Delta P_{\mathrm{v}i} \tag{6}$$

where $\Delta P_{\mathrm{m}i}$ is generator mechanical power output deviation, $T_{\mathrm{ch}i}$ is turbine time constant.

D. TIE-LINE POWER AND REGIONAL CONTROL DEVIATIONS

Ignoring the power loss generated during the transmission of the tie-line, the tie-line power is described as:

$$\Delta\dot{P}_{\mathrm{tie}-i} = 2\pi \sum_{j=1, i\neq 1}^{N} T_{ij}\Delta f_i \tag{7}$$

where $\Delta P_{\mathrm{tie}-i}$ is tie-line power change, T_{ij} is tie-line synchronizing coefficient.

The area control deviation δ_i is described as:

$$\delta_i = \chi_i\Delta f_i + \Delta P_{\mathrm{tie}-i} \tag{8}$$

where χ_i is frequency deviation factor.

E. FREQUENCY DEVIATION

The system load frequency deviation is shown as follows:

$$\Delta\dot{f}_i = -\frac{D_i}{M_i}\Delta f_i + \frac{1}{M_i}\Delta P_{\mathrm{m}i} - \frac{1}{M_i}\Delta P_{\mathrm{tie}-i} + \frac{1}{M_i}\Delta P_{\mathrm{pv}i} + \frac{1}{M_i}\Delta P_{\mathrm{b}i} - \frac{1}{M_i}\Delta P_{\mathrm{d}i} \tag{9}$$

where D_i is generator set damping factor, M_i is rotational inertia of the generator set, $\Delta P_{\mathrm{d}i}$ is system disturbances.

Combining Eq. (1)-(8), the system model is described as

$$\begin{aligned}\dot{\boldsymbol{x}}(t) &= \boldsymbol{A}\boldsymbol{x}(t) + \boldsymbol{B}u(t) + \boldsymbol{D}\boldsymbol{f}(t),\\ \boldsymbol{y}(t) &= \boldsymbol{C}\boldsymbol{x}(t),\end{aligned} \tag{10}$$

with shown at the bottom of the next page, where $\boldsymbol{x}(t)$ is system state, $\boldsymbol{A}$ is state matrix, $\boldsymbol{B}$ is system input matrix, $\boldsymbol{C}$ is output matrix,$\boldsymbol{y}(t)$ is system output matrix, $u(t)$ is control input and $\boldsymbol{D}$ is coefficient matrix.

Assume that the disturbances considered are bounded, it is written as:

$$\|f(t)\| \leq L_1, \left\|\dot{f}(t)\right\| \leq L_2,$$

where L_1, $L_2$are known constants.

III. MAIN CONCLUSION

A. PID CONTROLLER DESIGN

In interconnected power systems, PID controller takes the area control deviation δ_i as input variable. The output signal drives the actuator, which makes the steam valve of the turbine act according to the set direction.

The traditional PID controller has the advantages of simple structure and easy adjustment of parameters. However, PID controller cannot compensate for external interference effectively, which is difficult to cope with the complex power situation. In contrast, SMC is insensitive to external disturbances of the system, which can overcome the defects of PID control.

B. FTSMC DESIGN

First, when the upper and lower bound of the disturbances are known, to reduce the influence of PV grid connection uncertainty and system interference on frequency, the FTSMC is designed. For system (10), the fast terminal sliding surface is designed as:

$$s(t) = \dot{x}_1 + \alpha x_1 + \beta x_1^{\varepsilon}, \tag{11}$$

where $\alpha > 0, \beta > 0$ is the designed parameters, $\varepsilon = p/q$, $1 < \varepsilon < 2$, and p, q are both odd number.

To improve the dynamic performance of the system, the sliding mode convergence law is designed as follows:

$$\dot{s}(t) = k_1 s(t) + k_2 |s(t)|^{\varepsilon} \operatorname{sgn}(s(t)), \tag{12}$$

where k_1, k_2, ε are the convergence law parameters to be designed.

Further, the FTSMC can be designed as follows:

$$u(t) = -\frac{1}{H_1}\left\{H_2 + k_1 s(t) + k_2 |s(t)|^{\varepsilon} \operatorname{sgn}(s(t)) + \left[\left(\frac{D_i}{M_i^2} - \frac{\alpha}{M_i}\right) L_1 + \frac{1}{M_i} L_2\right] \operatorname{sgn}(s(t))\right\}, \tag{13}$$

$$\boldsymbol{x}(t) = [\boldsymbol{x}_1(t)\boldsymbol{x}_2(t)\,\boldsymbol{x}_3(t)\cdots\,\boldsymbol{x}_n(t)]^{\mathrm{T}},$$
$$\boldsymbol{y}(t) = [\boldsymbol{y}_1(t)\boldsymbol{y}_2(t)\,\boldsymbol{y}_3(t)\cdots\boldsymbol{y}_n(t)]^{\mathrm{T}},$$
$$\boldsymbol{x}_i(t) = \left[\Delta f_i\ \Delta P_{\mathrm{m}i}\Delta P_{\mathrm{v}i}\Delta P_{\mathrm{tie}-i}\int \delta_i \Delta P_{\mathrm{b}i}\Delta P_{\mathrm{pv}i}\Delta P_{\mathrm{p}i}\right]^{\mathrm{T}},$$
$$\boldsymbol{y}_i(t) = \left[\Delta f_i \int \delta_i\right]^{\mathrm{T}},$$
$$\boldsymbol{f}(t) = \Delta P_{\mathrm{d}i},$$

$$\boldsymbol{A}_{ii} = \begin{bmatrix} -\frac{D_i}{M_i} & \frac{1}{M_i} & 0 & -\frac{1}{M_i} & 0 & \frac{1}{M_i} & \frac{1}{M_i} & 0 \\ 0 & -\frac{1}{T_{\mathrm{ch}i}} & \frac{1}{T_{\mathrm{ch}i}} & 0 & 0 & 0 & 0 & 0 \\ -\frac{1}{R_i T_{\mathrm{g}i}} & 0 & -\frac{1}{T_{\mathrm{g}i}} & 0 & 0 & 0 & 0 & 0 \\ 2\pi \sum_{j=1, i\neq 1}^{N} T_{ij} & 0 & 0 & 0 & 0 & 0 & 0 & 0 \\ \chi_i & 0 & 0 & 1 & 0 & 0 & 0 & 0 \\ 0 & 0 & 0 & 0 & 0 & -\frac{1}{T_{\mathrm{b}i}} & 0 & 0 \\ 0 & 0 & 0 & 0 & 0 & 0 & -\lambda_3 & \lambda_2 - \lambda_1 \\ 0 & 0 & 0 & 0 & 0 & 0 & 0 & -\lambda_1 \end{bmatrix}$$

$$\boldsymbol{A}_{ij} = \begin{bmatrix} 0 & 0 & 0 & 0 & 0 & 0 & 0 & 0 \\ 0 & 0 & 0 & 0 & 0 & 0 & 0 & 0 \\ 0 & 0 & 0 & 0 & 0 & 0 & 0 & 0 \\ 2\pi \sum_{j=1, i\neq 1}^{N} T_{ij} & 0 & 0 & 0 & 0 & 0 & 0 & 0 \\ 0 & 0 & 0 & 0 & 0 & 0 & 0 & 0 \\ 0 & 0 & 0 & 0 & 0 & 0 & 0 & 0 \\ 0 & 0 & 0 & 0 & 0 & 0 & 0 & 0 \\ 0 & 0 & 0 & 0 & 0 & 0 & 0 & 0 \end{bmatrix}, \quad \boldsymbol{B} = \begin{bmatrix} 0 \\ 0 \\ \frac{\alpha_{\mathrm{g}i}}{T_{\mathrm{g}i}} \\ 0 \\ 0 \\ \frac{\alpha_{\mathrm{b}i} k_{\mathrm{b}i}}{T_{\mathrm{b}i}} \\ k_{\mathrm{p}i}\alpha_{\mathrm{pv}i} \\ k_{\mathrm{p}i}\alpha_{\mathrm{pv}i} \end{bmatrix},$$

$$\boldsymbol{C} = \begin{bmatrix} 1 & 0 & 0 & 0 & 0 & 0 & 0 & 0 \\ 0 & 0 & 0 & 0 & 1 & 0 & 0 & 0 \end{bmatrix}, \quad \boldsymbol{D} = \begin{bmatrix} -\frac{1}{M_i} \\ 0 \\ 0 \\ 0 \\ 0 \\ 0 \\ 0 \\ 0 \end{bmatrix},$$

where

$$H_1 = \frac{\alpha_{\mathrm{bi}} k_{bi}}{M_i T_{\mathrm{bi}}} + \frac{k_{\mathrm{pi}} \alpha_{\mathrm{pv}i}}{M_i},$$

$$\begin{aligned} H_2 = & \left[\left(\frac{D_i}{M_i} \right)^2 - \frac{2\pi T_{ij}}{M_i} - \frac{\alpha D_i}{M_i} \right] x_1 \\ & + \left(\frac{D_i}{M_i^2} - \frac{1}{M_i T_{\mathrm{ch}i}} + \frac{\alpha}{M_i} \right) x_2 + \frac{1}{M_i T_{\mathrm{ch}i}} x_3 \\ & + \left(\frac{D_i}{M_i^2} - \frac{\alpha}{M_i} \right) x_4 + \left(-\frac{D_i}{M_i^2} - \frac{1}{M_i T_{\mathrm{bi}}} + \frac{\alpha}{M_i} \right) x_6 \\ & + \left(-\frac{D_i}{M_i^2} - \frac{\lambda_3}{M_i} + \frac{\alpha}{M_i} \right) x_7 + \frac{\lambda_2 - \lambda_1}{M_i} x_8 \\ & + \left(\frac{D_i}{M_i^2} - \frac{\alpha}{M_i} \right) f(t) - \frac{1}{M_i} \dot{f}(t) + \beta \varepsilon x_1^{\varepsilon - 1} \dot{x}_1 \Bigg]. \end{aligned}$$

The Lyapunov function is chosen as:

$$V(t) = \frac{1}{2} s^2(t), \tag{14}$$

The derivative of (14) is written as

$$\dot{V}(t) = \frac{1}{2} s(t) \dot{s}(t), \tag{15}$$

Deriving Eq. (11), it yields

$$\begin{aligned} \dot{s}(t) &= \ddot{x}_1 + \alpha \dot{x}_1 + \beta \varepsilon x_1^{\varepsilon - 1} \dot{x}_1 \\ &= -\frac{D_i}{M_i} \dot{x}_1 + \frac{1}{M_i} \dot{x}_2 - \frac{1}{M_i} \dot{x}_4 + \frac{1}{M_i} \dot{x}_6 + \frac{1}{M_i} \dot{x}_7 - \frac{1}{M_i} \dot{f}(t) \\ &\quad + \alpha \left(-\frac{D_i}{M_i} x_1 + \frac{1}{M_i} x_2 - \frac{1}{M_i} x_4 + \frac{1}{M_i} x_6 \right. \\ &\quad \left. + \frac{1}{M_i} x_7 - \frac{1}{M_i} \dot{f}(t) \right) + \beta \varepsilon x_1^{\varepsilon - 1} \dot{x}_1. \end{aligned} \tag{16}$$

Combining Eq. (13) and (16), Eq. (14) is written as:

$$\begin{aligned} & \dot{V}(t) \\ & = s(t) \left[\left(\frac{D_i}{M_i^2} - \frac{\alpha}{M_i} \right) f(t) - \frac{1}{M_i} \dot{f}(t) - k_1 s(t) - k_2 |s(t)|^{\varepsilon} \right. \\ & \quad \left. \times \operatorname{sgn}(s(t)) - \left(\frac{D_i}{M_i^2} - \frac{\alpha}{M_i} \right) L_1 \operatorname{sgn}(s(t)) - \frac{1}{M_i} L_2 \operatorname{sgn}(s(t)) \right] \\ & \le -k_1 s^2(t) - k_2 |s(t)|^{\varepsilon + 1} + \left(\frac{D_i}{M_i^2} - \frac{\alpha}{M_i} \right) L_1 |s(t)| \\ & \quad + \frac{1}{M_i} L_2 |s(t)| - \left(\frac{D_i}{M_i^2} - \frac{\alpha}{M_i} \right) L_1 |s(t)| - \frac{1}{M_i} L_2 |s(t)| \\ & \le -k_1 s^2(t) - k_2 |s(t)|^{\varepsilon + 1} \end{aligned} \tag{17}$$

From the above analysis, it is shown that, when the disturbances satisfy the condition that $\|f(t)\| \le L_1$ and $\left\|\dot{f}(t)\right\| \le L_2$, $\dot{V}(t) < 0$ is obtained.

C. AFTSMC DESIGN

To reduce the dependence on system disturbances bounds, the controller is designed as

$$\begin{aligned} u(t) = -\frac{1}{H_1} \Bigg\{ & H_2 + k_1 s(t) + k_2 |s(t)|^{\varepsilon} \operatorname{sgn}(\mathrm{s(t)}) \\ & + \left[\left(\frac{D_i}{M_i^2} - \frac{\alpha}{M_i} \right) \hat{L} + \frac{1}{M_i} L_2 \right] \operatorname{sgn}(\mathrm{s(t)}) \Bigg\}, \end{aligned} \tag{18}$$

where $\hat{L}$ is estimated value of the upper bound of disturbances L, estimation error $\tilde{L} = L - \hat{L}$. The adaptive law is designed as:

$$\dot{\hat{L}} = \left(\frac{D_i}{M_i^2} - \frac{\alpha}{M_i} \right) s(t) \tag{19}$$

Next, the Lyapunov function is chosen as

$$V(t) = \frac{1}{2} s^2(t) + \frac{1}{2} \tilde{L}^2 \tag{20}$$

By deriving Eq. (20), it is obtained that

$$\begin{aligned} & \dot{V}(t) \\ & = s(t) \left[\left(\frac{D_i}{M_i^2} - \frac{\alpha}{M_i} \right) f(t) - \frac{1}{M_i} \dot{f}(t) - k_2 |s(t)|^{\varepsilon} \operatorname{sgn}(s(t)) \right. \\ & \quad \left. - k_1 s(t) - \left(\frac{D_i}{M_i^2} - \frac{\alpha}{M_i} \right) \hat{L} \operatorname{sgn}(s(t)) - \frac{1}{M_i} L_2 \operatorname{sgn}(s(t)) \right] \\ & \quad - \tilde{L} \dot{\hat{L}} \\ & \le -k_1 s^2(t) - k_2 |s(t)|^{\varepsilon + 1} + \left(\frac{D_i}{M_i^2} - \frac{\alpha}{M_i} \right) \left(\tilde{L} + \hat{L} \right) s(t) \\ & \quad - \left(\frac{D_i}{M_i^2} - \frac{\alpha}{M_i} \right) \hat{L} |s(t)| - \tilde{L} \dot{\hat{L}} \\ & \le -k_1 s^2(t) - k_2 |s(t)|^{\varepsilon + 1} + \left(\frac{D_i}{M_i^2} - \frac{\alpha}{M_i} \right) \tilde{L} s(t) \\ & \quad + \left(\frac{D_i}{M_i^2} - \frac{\alpha}{M_i} \right) \hat{L} |s(t)| - \left(\frac{D_i}{M_i^2} - \frac{\alpha}{M_i} \right) \hat{L} |s(t)| - \tilde{L} \dot{\hat{L}} \\ & \le -k_1 s^2(t) - k_2 |s(t)|^{\varepsilon + 1} + \tilde{L} \left[\left(\frac{D_i}{M_i^2} - \frac{\alpha}{M_i} \right) s(t) - \dot{\hat{L}} \right] \end{aligned} \tag{21}$$

Substituting Eq. (19) into Eq. (21), one obtains

$$\dot{V}(t) \le -k_1 s^2(t) - k_2 |s(t)|^{\varepsilon + 1} < 0 \tag{22}$$

From Eq. (23), it can be derived that, when the adaptive law is $\dot{\hat{L}} = \left(\frac{D_i}{M_i^2} - \frac{\alpha}{M_i} \right) s(t)$, $\dot{V}(t) < 0$ can be guaranteed, which means that $s(t) = 0$ is satisfied under AFTSMC. When $s(t) = 0$, according to Eq. (11), we have

$$\dot{x}_1 = -\alpha x_1 - \beta x_1^{\varepsilon} \tag{23}$$

Further, define the Lyapunov function as

$$V(t) = \frac{1}{2} x_1^2 \tag{24}$$

TABLE 1. Area system parameters.

Parameters	Area 1	Area 2	Parameters	Area 1	Area 2
T_{chi}	0.35	0.4	δ_i	0.4	0.4
T_{gi}	0.08	0.09	λ_{1i}	99.5	98
R_i	5	5	λ_{2i}	-50	-50
β_i	0.4	0.4	λ_{3i}	0.5	0.5
D_i	0.02	0.01	k_{pi}	120	120
M_i	0.3	0.3	k_{bi}	10	15
T_{ij}	0.2	0.22	T_{bi}	1	1

By deriving Eq. (24), it yields:

$$\begin{aligned}\dot{V}(t) &= x_1\dot{x}_1 \\ &= x_1(-\alpha x_1 - \beta x_1^{\varepsilon}) \\ &= -\alpha x_1^2 - \beta x_1^{\varepsilon+1}\end{aligned} \tag{25}$$

Since $0 < \varepsilon < 1$, $1 < \varepsilon + 1 < 2$, $\dot{V}(t) < 0$ is guaranteed, which shows that x_1 converges to zero in finite time. Combining with Eq. (25), $\dot{V}(t)$ and the convergence time t_s is written as:

$$\begin{cases}\dot{V}(t) \le -aV(t) - bV^{\eta}(t) \\ t_s = \dfrac{1}{a(1-b)}\ln\dfrac{b + aV^{1-\eta}(0)}{b}\end{cases} \tag{26}$$

where $a = 2\alpha$, $b = 2^{\eta}\beta$, $\eta = \frac{1}{2}(\varepsilon + 1)$.

IV. SIMULATIONS

In this section, interconnected power systems with PV and ESS in two areas are considered. The simulations of three cases are carried out, mainly including: a) comparison with the conventional PID control strategy, b) comparison with and without ESS and c) simulation results compared with different controller parameters.

Assuming that system with disturbances at $t \ge 0$. The magnitude of the disturbances in two areas takes the values as $\Delta P_{d1} = \Delta P_{d2} = \sin(t)$. In the two areas, ESS proportional factor $\alpha_{e1} = 0.3, \alpha_{e2} = 0.4$, turbine proportional factor $\alpha_{g1} = 0.6, \alpha_{g2} = 0.5$, PV proportional factor $\alpha_{pv1} = 0.1$, $\alpha_{pv2} = 0.1$. The system parameters of the two areas are shown in Table 1.

A. COMPARISON OF SIMULATION RESULTS OF PID, FTSMC AND AFTSMC

Firstly, when ESS is participated in frequency modulation, the convergence of load frequency deviation Δf_i under PID, FTSMC, and AFTSMC is considered. The controller parameters are shown in Table 2 and Table 3, respectively. The simulation results of the power systems with two areas are shown in Fig. 2.

As shown from Fig. 2 and Table 2, it is seen that under the configuration of ESS in the power systems, the load frequency deviations Δf_i of the three control methods are different. The maximum values of frequency deviation under PID,

TABLE 2. PID controller parameters.

Symbol	Area 1	Area 2
K_p	0.5	0.4
K_i	2	1.5
K_d	0.05	0.07

TABLE 3. FTSMC, AFTSMC parameters.

Symbol	Area 1	Area 2
α	2	1.5
β	0.5	0.6
ε	0.5	0.6
k_1	5	3
k_2	0.5	0.8

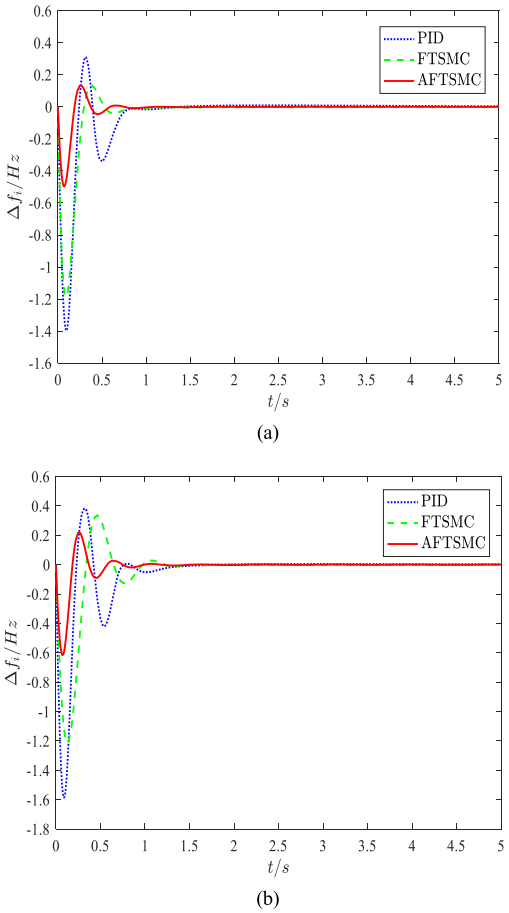

FIGURE 2. (a) Simulation comparison of PID, FTSMC and AFTSMC in area 1. (b) Simulation comparison of PID, FTSMC and AFTSMC in area 2.

FTSMC, and AFTSMC are -1.5858Hz, -1.1875Hz, and -0.6154Hz, respectively. In addition, by applying AFTSMC, fluctuations of Δf_i are further reduced in stabilization process. In comparison, the FTSMC and AFTSMC can reduce the frequency deviation during area interconnection effectively, which enhances the performance of the system.

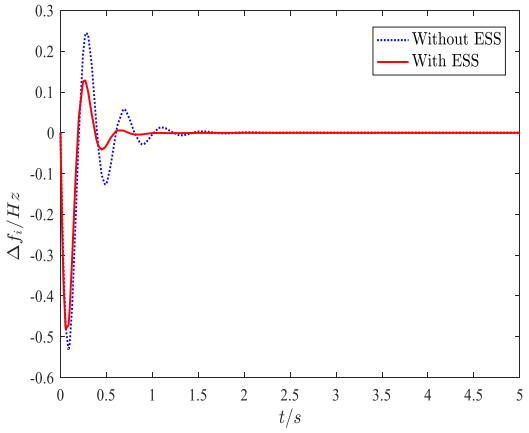

(a)

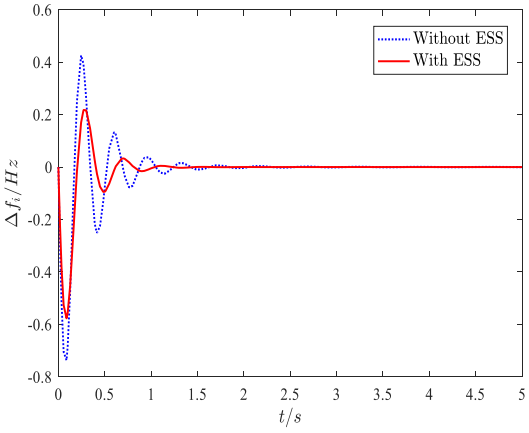

(b)

FIGURE 3. (a) Load frequency deviation with and without ESS under AFTSMC in area 1. (b) Load frequency deviation with and without ESS under AFTSMC in area 2.

B. COMPARISON RESULTS WITH AND WITHOUT ESS

In this section, experiments are carried out to illustrate the frequency modulation effect of ESS. Under the condition that the system model parameters remain unchanged, the simulation is performed with AFTSMC with two cases that with or without ESS in the system. The simulation results are shown in Fig. 3.

In Fig. 3, the simulation results indicate that the variation of the load frequency deviation Δf_i with and without ESS. Compared with the case without ESS in the system, when ESS is applied, the overshoot of load frequency deviation Δf_i is smaller. Meanwhile, the number of oscillations is reduced, enabling the stabilization be realized in shorter time. Therefore, it is shown that, when ESS and AFTSMC work in coordination, the fluctuation of the area interconnection systems is further reduced. The feasibility and effectiveness of ESS participation in frequency control is verified.

C. THE RESULTS OF FREQUENCY DEVIATION WITH DIFFERENT ε

In Eq. (11), ε is the index of the higher order term in sliding surface $s(t) = \dot{x}_1 + \alpha x_1 + \beta x_1^{\varepsilon}$. Different from the general

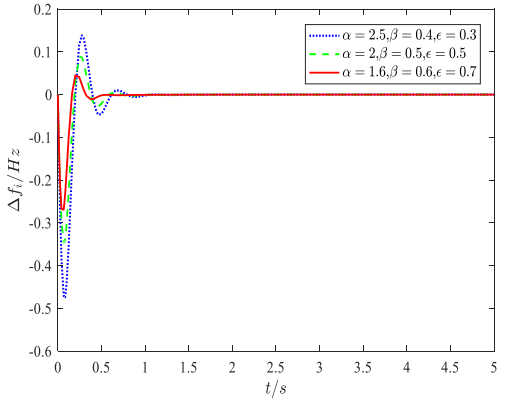

(a)

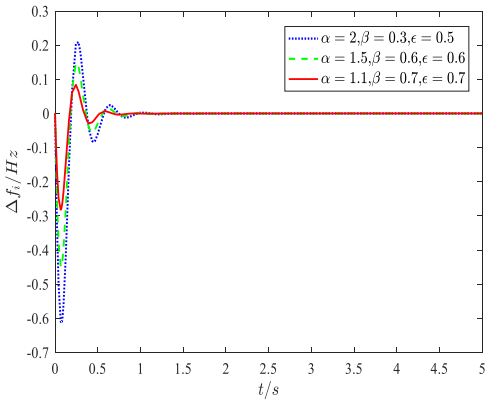

(b)

FIGURE 4. (a) Load frequency deviation Δf_i with different ε in area 1. (b) Load frequency deviation Δf_i with different ε in area 2.

TABLE 4. Simulation data of different α, β and ε.

Comparison Object	Parameters			Frequency deviation maximum $\Delta f_{i\max}$/Hz
	α	β	ε	
Δf_1	2.5	0.4	0.3	-0.4695
	2	0.5	0.5	-0.3464
	1.6	0.6	0.7	-0.2694
Δf_2	2	0.3	0.5	-0.6086
	1.5	0.6	0.6	-0.4493
	1.1	0.7	0.7	-0.2894

TSMC, the purpose of the higher order term is to speed up the convergence of the system state. Meanwhile, according to Eq. (26), when parameters α, β and ε are changed, the convergence progress of the system is also influenced. Next, to compare the control effects, based on the AFTSMC parameters in Table 3, the control parameters are selected as in Table 4. The simulation results are shown in Fig. 4.

According to Eq. (26), when the parameter of β, ε increase and α decrease, the maximum value of frequency deviation $\Delta f_{i\max}$ decrease. In addition, the convergence time t_s reduce. Combining Fig. 4 and Table 4, it is seen that when the two area parameters are chosen as $\alpha_1 = 1.6$, $\beta_1 = 0.6$, $\varepsilon_1 = 0.7$, $\alpha_2 = 1.6$, $\beta_2 = 0.6$, $\varepsilon_2 = 0.7$, the $\Delta f_{1\max}$ and $\Delta f_{2\max}$

decrease by -0.2694 Hz and -0.2894 Hz, respectively. The fluctuations of are also reduced.

In contrast, when the parameters of β, ε decrease and α increase, $\Delta f_{i\max}$ and t_s will increase. In the simulation results, when the two area parameters are chosen as $\alpha_1 = 2.5$, $\beta_1 = 0.4$, $\varepsilon_1 = 0.3$, $\alpha_2 = 2$, $\beta_2 = 0.3$, $\varepsilon_2 = 0.5$, $\Delta f_{i\max}$ also increases to -0.4965 Hz and -0.6086 Hz, respectively. During the convergence process of Δf_i, its fluctuation also increases. Through the simulation results in this section, it is illustrated that we can obtain control effects corresponding to the theoretical analysis by selecting appropriate controller parameters α, β and ε, which further improve the performance of the system.

V. CONCLUSION

In this paper, considering the grid integration of renewable generation energy and the increasing scale of the power grid, LFC of interconnected power systems containing PV and ESS is studied. To compensate the uncertainty of renewable energy generation and the influence of disturbances, a control strategy of ESS and FTSMC cooperatively is proposed. Based on the model of LFC containing PV and ESS, FTSMC and AFTSMC are designed. By introducing the adaptive law, the dependence on the upper bound of the system disturbances is reduced with the designed AFTSMC. Furthermore, when the ESS is involved in LFC, it has good suppression effect on load frequency deviation, which improves the performance of the power systems. However, other types of renewable energy generation and numbers of areas are not considered. In the future research, when multiple regions are interconnected, the problem of LFC for multiple renewable energy generation will be further investigated.

REFERENCES

[1] M. Ding, W. Wang, X. Wang, Y. Song, D. Chen, and M. Sun, "A review on the effect of large-scale PV generation on power systems," *Proc. CSEE*, vol. 34, no. 1, pp. 1–14, Jan. 2014.

[2] X. X. Zhou, Z. X. Lu, Y. M. Liu, and S. Y. Chen, "Development models and key technologies of future grid in China," *Proc. CSEE*, vol. 23, no. 29, pp. 4999–5008, Oct. 2014.

[3] M. Ourahou, W. Ayrir, B. EL Hassouni, and A. Haddi, "Review on smart grid control and reliability in presence of renewable energies: Challenges and prospects," *Math. Comput. Simul.*, vol. 167, pp. 19–31, Jan. 2020.

[4] J. G. Yao, S. C. Yang, and M. H. Shan, "Reflections on operation supporting system architecture for future interconnected power grid," *Autom. Electr. Power Syst.*, vol. 37, no. 21, pp. 52–59, Nov. 2013.

[5] P. H. Xie, C. Wang, and P. H. Liu, "Application of joint frequency regulation technology of energy storage and thermal power in China southern power grid," *Autom. Electr. Power Systems.*, vol. 45, no. 4, pp. 172–179, Feb. 2021.

[6] C. Song, X. H. Wang, and H. Y. Li, "Interconnected power system load frequency control based on super-capacitor," *Control Eng. China*, vol. 26, no. 6, pp. 1158–1162, Jun. 2019.

[7] D. Xu, J. Liu, and X. Yan, "A novel adaptive neural network constrained control for a multi-area interconnected power system with hybrid energy storage," *IEEE Trans. Ind. Electron.*, vol. 65, no. 8, pp. 6625–6634, Aug. 2019.

[8] M. Elsisi, M. Aboelela, M. Soliman, and W. Mansour, "Design of optimal model predictive controller for LFC of nonlinear multi-area power system with energy storage devices," *Electric Power Compon. Syst.*, vol. 46, nos. 11–12, pp. 1300–1311, Jul. 2018.

[9] E. Tian and C. Peng, "Memory-based event-triggering H_∞ load frequency control for power systems under deception attacks," *IEEE Trans. Cybern.*, vol. 50, no. 11, pp. 4610–4618, Nov. 2020.

[10] K. Wang, E. Tian, J. Liu, L. Wei, and D. Yue, "Resilient control of networked control systems under deception attacks: A memory-event-triggered communication scheme," *Int. J. Robust Nonlinear Control*, vol. 30, no. 4, pp. 1534–1548, Mar. 2020.

[11] H. Shan, J. He, and L. X. Fan, "Research on fractional order PID control of regional load frequency of pumped storage power station," *Power Syst. Technol.*, vol. 39, no. 3, pp. 1410–1418, Apr. 2020.

[12] M. Elsisi, "New variable structure control based on different meta-heuristics algorithms for frequency regulation considering nonlinearities effects," *Int. Trans. Electr. Energy Syst.*, vol. 30, no. 7, Jul. 2020, Art. no. e12428.

[13] M. Elsisi, N. Bazmohammadi, J. M. Guerrero, and M. A. Ebrahim, "Energy management of controllable loads in multi-area power systems with wind power penetration based on new supervisor fuzzy nonlinear sliding mode control," *Energy*, vol. 221, Apr. 2021, Art. no. 119867.

[14] Y. Mi, X. Z. Hao, and H. Y. Liu, "Multi-area power system with wind power and energy storage system load frequency control based on sliding model control," *Control Decis.*, vol. 34, no. 2, pp. 437–444, Aug. 2016.

[15] D. G. Jiang, L. J. Lv, and S. H. Pan, "Fast terminal sliding mode active disturbance rejection control for trajectory tracking of mobile robot," *Control Eng. China*, to be published, doi: 10.14107/j.cnki.kzgc.20200059.

[16] X. L. Wang, L. L. Qin, and H. Gu, "Improved fast terminal sliding mode control based on fractional order calculus for permanent magnet synchronous motor," *Proc. CSU-EPSA*, to be published, doi: 10.19635/j.cnki.csu-epsa.000467.

[17] J. Q. Yang, Y. X. Gao, and Y. T. Chen, "Disturbance observer-based terminal sliding mode controller design for uncertain nonlinear systems," *Control Decis.*, vol. 35, no. 1, pp. 155–160, Jan. 2020.

[18] L. L. Yu, Z. X. Kuang, and Z. J. Wang, "Intelligent vehicle platoon lateral and longitudinal control based on finite-time sliding mode control," *Control Theory Appl.*, to be published. [Online]. Available: https://kns.cnki.net/kcms/detail/44.1240.TP.20210112.1248.012.html, doi: 10.7641/CTA.2020.00389.

[19] E. Ganji, R. K. Moghaddam, A. Toloui, and M. Taghizadeh, "A new control method for leveling output frequency fluctuations in an autonomous PV/FC/UC network with maximum power point tracking of the photovoltaic system," *J. Intell. Fuzzy Syst.*, vol. 27, no. 4, pp. 1949–1962, 2014.

[20] D. Qian and G. Fan, "Neural-network-based terminal sliding mode control for frequency stabilization of renewable power systems," *IEEE/CAA J. Automatica Sinica*, vol. 5, no. 3, pp. 706–717, May 2018.

[21] A. Bagheri, A. Jabbari, and S. Mobayen, "An intelligent ABC-based terminal sliding mode controller for load-frequency control of islanded micro-grids," *Sustain. Cities Soc.*, vol. 64, Jan. 2021, Art. no. 102544, doi: 10.1016/j.scs.2020.102544.

[22] G. D. Fan, S. L. Liu, and J. Pei, "Load frequency coordinated optimization control of hybrid power generation system consisted of PV, thermal power and energy storage," *Proc. CSU-EPSA*, vol. 32, no. 12, pp. 134–143, Aug. 2020.

ZHENGHAO WANG received the B.E. degree in electrical engineering and automation from the Qilu University of Technology, Shandong, China, in 2019. He is currently pursuing the M.Sc. degree with Shanghai Dianji University, Shanghai, China. His research interests include power systems and automation.

YONGHUI LIU received the Ph.D. degree from East China University of Science and Technology. In 2014, she joined the School of Electrical Engineering, Shanghai Dianji University, where she is currently an Associate Processor. Her research interests cover sliding mode control, switched systems, and fault tolerant control.